PHYSICAL REVIEW E **94**, 040401(R) (2016)

Types and concentrations of metal ions affect local structure and dynamics of RNA

Jun Wang and Yi Xiao*

Biomolecular Physics and Modeling Group, School of Physics, Huazhong University of Science and Technology, Wuhan 430074, Hubei, China

(Received 14 July 2016; published 24 October 2016)

The roles that metal ions play in the structure and dynamics of RNA molecules are long-standing problems that have been studied extensively but are still not well understood. Here we show that metal ions have distributions around RNA molecules that strongly depend on the types and concentrations of the metal ions and also the electrostatic surface of the molecule. In particular, the ion distributions may not balance all the local electronegativity of the molecule. These ion distributions do not only greatly affect local structures but also lead to different local dynamics of RNA. We studied the effects of different ion solutions on the structure and dynamics of RNA by taking the preQ$_1$ riboswitch aptamer domain as an illustrative example and using molecular dynamics simulations. Since the local structures and dynamics of RNAs are important to their functions, our results also indicate that the selection of proper ion conditions is necessary to model them correctly, in contrast to the use of diverse ion solutions in current molecular dynamics simulations.

DOI: 10.1103/PhysRevE.94.040401

Metal ions play crucial roles in the structure and dynamics of RNAs, besides net neutralizing their strong electronegativity [1]. These roles are long-standing problems that have been discussed extensively but they are still not well understood [2–7]. For example, some studies reported that the types of ions did not affect the dynamics significantly while some showed the opposite [2]. It was also shown that the local conformations of RNA samples depend on the types and concentrations of the metal ions [8]. Therefore, metal ions do not just balance the electronegativity of RNAs but may play other rules in their structures and dynamics and need to be investigated further.

To understand the roles of metal ions, both experimental and theoretical (or computational) approaches are needed [2,9–11]. However, these two approaches usually use different ion solutions. For example, experimental studies frequently used buffers containing KCl and/or $MgCl_2$ to prepare the RNA samples [8,12–17], which is close to an intracellular environment since K^+ is the dominant cation in the cell. On the other hand, computational studies used different ion solutions containing net-neutralizing Na^+,K^+, or Mg^{2+} ions with or without excess salts, even for the same molecule [2,10,18–27]. The molecular dynamics simulations using these different ion solutions have captured some aspects of the structures and dynamics of RNA, but whether they can give a consistent and complete description of the structures and dynamics of RNA also needs to be addressed further.

Here we take a preQ$_1$ riboswitch aptamer domain (simply, PRAD) from *Bacillus subtilis* as an illustrative example to investigate the effects of different ion solutions by using molecular dynamics (MD) simulations. The reason for studying PRAD is that it is a small, natural aptamer domain consisting of 36 nucleotides but also containing the most basic structural units, including hairpins, duplexes, junctions, and pseudoknots [8,13,15]. In particular, for the PRAD, the crystal and NMR solution structures as well as the dynamics have been measured [8,28]. We show that in different ion solutions the global stabilities of PRAD are similar but the local structures and dynamics are different.

We have performed ten sets of molecular dynamics simulations on a type-I preQ$_1$-bound riboswitch aptamer domain (Table I). For each set, three independent 600 ns trajectories were simulated using the pmemd.cuda [29–31] program in the assisted model building with energy refinement (AMBER14) software package and the ff14SB force field [32] for RNA, denoted as ff99 + bsc0 + χ_{OL3}, which is a refined force field parameters 99 with a correction for α/γ backbone torsion (bsc0) [33] and a correction for the glycosidic torsion (χ_{OL3}) [34]. The starting structure was the first of 20 NMR structures of the preQ$_1$ -bound riboswitch aptamer domain [Protein Data Bank (PDB) ID: 2L1V [13], Fig. 1]. ANTECHAMBER [35,36] and the general AMBER force field (GAFF) [36] were used to model the preQ$_1$ ligand. The partial charges for the ligand atoms were calculated using the Austin Model 1 bond charge correction (AM1-bcc) model [37]. tLEaP [38] was used to generate an explicitly solvated RNA structure with a TIP3P water model and the periodic boundary condition by adding an octahedral box with a 9.0 Å pad distance. Here tLEaP and ANTECHAMBER are programs of AMBER14 for preparation of the parameter and coordinate files for proteins and nucleic acids and the parameter sets for small molecules, respectively.

The parameters for Na^+,K^+, and Cl^- ions are those provided by Joung and Cheatham *et al.* with Lennard-Jones (LJ) potential well depths of 0.0874393, 0.1936829, and 0.0355910 kcal/mol and with radii of 1.369, 1.705, and 2.513 Å, respectively [39]. The parameters for magnesium ions are the one provided by Li and Merz *et al.* [40] with a LJ potential well depth of 0.00396 kcal/mol and an ion radius of 1.284 Å, respectively.

Before the simulations, all the systems were minimized by the use of 3000 steps of the descent method and 3000 steps of conjugate gradient optimization. During the first 3000 steps of minimization, the entire riboswitch and ligand were restrained by a harmonic potential (500 kcal/mol/Å^2) to their initial positions to let the water molecules and ions diffuse. In the second 3000 steps of minimization, all atoms were free to move. Then, the systems were heated from 0 to 300 K in 200 ps with the NVT ensemble to avoid the formation of a vacuum

*Author to whom correspondence should be addressed: yxiao@mail.hust.edu.cn

TABLE I. Summary of simulations.

Set ID	Ion solution
1	No ions
2	Neutralizing Na^+
3	Neutralizing K^+
4	Neutralizing Mg^{2+}
5	Neutralizing Na^+, extra 0.3M NaCl
6	Neutralizing Na^+, extra 0.3M KCl
7	Neutralizing Na^+, extra 0.15M $MgCl_2$
8	Neutralizing K^+, extra 0.3M NaCl
9	Neutralizing K^+, extra 0.3M KCl
10	Neutralizing K^+, extra 0.15M $MgCl_2$

bubble in the NPT ensemble. After that, the systems were equilibrated in 1 ns before a production run. In the production run, we used a 2 fs time step with the help of the SHAKE algorithm [41]. The Langevin thermostat was used to control the temperature using a collision frequency of 1.0/ps [42], and the particle mesh Ewald (PME) [43] method was used to calculate the long-range electrostatic potential. The cutoff distance for the van der Waals potential is 10.0 Å.

After the simulations, all trajectories were analyzed by the CPPTRAJ program [44] in the AMBER14 software package. The root mean square deviation (RMSD) was calculated with all heavy atoms in the riboswitch aptamer relative to the first NMR structure. We wrote a program to analyze the ion distribution in space. Our procedure is as follows: (a) Strip the water molecules and align all the RNA structures in trajectories to the native structure; (b) find the maximum and minimum in three directions with three independent trajectories in all atoms; (c) grid the space with a grid size of 0.5 Å; (d) treat each ion atom as a sphere and then count the times that the atomic spheres occur in each grid; and (e) divide the number of times by the total frames in all structures and we get an open visualization data explorer (openDX) file to denote the distribution of metal ions. After that, PYMOL [28] was used to color the volume space and ray of our structures. All the data graphs were plotted by the Python package called MATPLOTLIB [45] and R [46] inner graph systems. The electrostatic potential of the PRAD was calculated by Delphi [47].

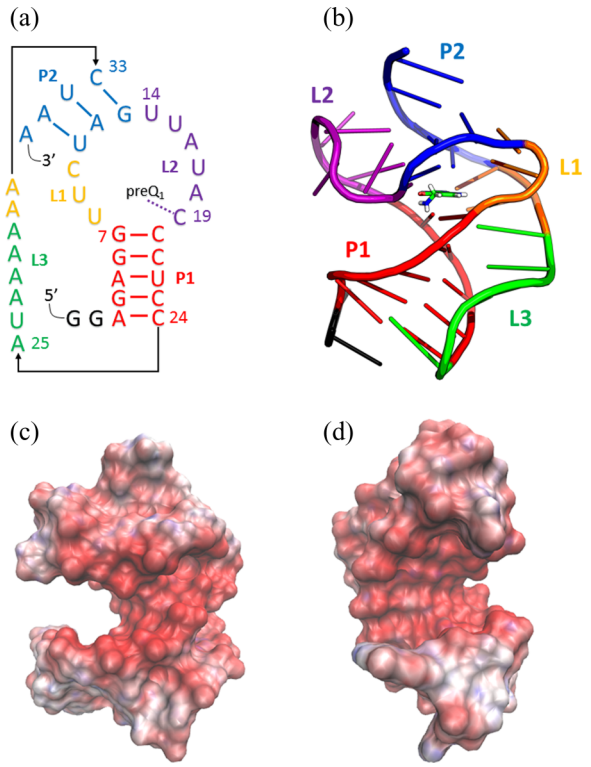

FIG. 1. Structures and electrostatic surface of the bound $preQ_1$ riboswitch aptamer domain (PDB ID: 2L1V). (a) Secondary and (b) tertiary structures; (c) and (d) different views of the electrostatic surface. In (a) and (b) different components (P1, P2, L1, L2, and L3) are coded in color and the ligand $preQ_1$ is represented by a stick model. In (c) and (d) the electrostatic potential increases from red (dark) to blue (light).

Figure 1 shows the secondary and tertiary structures and electrostatic surface of the bound PRAD (PDB ID: 2L1V) [13]. The structure of the aptamer is an H-type pseudoknot with two stems (P1 and P2) and three loops (L1, L2, and L3). An NMR experiment [8,13] shows that the entire molecule is very stable in the bound state. However, the conformational flexibilities or dynamics of different parts of the molecule are different. The lower part (LP) P1-L3 and its components (P1 and L3) are very stable, even without the ligand, while the upper part (UP) L1-L2-P2 is relatively flexible. In particular, NMR relaxation measurements revealed the following [8]: (1) L2 is the highly dynamic region of the $preQ_1$ -bound aptamer on a ps–ns time scale but it has no motions on the longer μs–ms time scale; (2) L1 are remarkably stable on a ps–ns time scale but they (including U12 from P2 but not U8 from L1) undergo concerted motions on the μs–ms time scale. P2 is also flexible due to the weak interaction of the terminal base pairing. In the following we will study the ps–ns time-scale dynamics of the bound PRAD in different ion solutions.

The ion distributions in nine different ion solutions are shown in Fig. 2. We find that metal ions behave in a completely different way, although they mainly stay in the groove between the LP and UP parts (ligand-binding pocket) because this region has strong electronegativity given by the backbone of the RNA molecule (Fig. 1). Na^+ ions do not diffuse around the entire molecule but tend to go deep into the binding-pocket groove and distribute in its bottom. On the other hand, K^+ ions mainly distribute in the upper part of the binding-pocket groove and around the molecule and have a larger diffusion rate than Na^+ ions. Mg^{2+} ions distribute within the whole binding-pocket groove but bind some sites with higher probability, such as the results of previous studies [11]. They are almost localized and strongly interact with the backbone phosphate groups where they stay (Fig. 3). These different behaviors of the metal ions clearly depend on the types (radius and charge) and concentrations of the ions and are in agreement with previous results [48]. Furthermore, the ion distributions become smoother as the ion concentrations increase [Figs. 2(d)–2(i)].

The different distributions of metal ions affect the local structures of the molecule. For example, in the cases where the ions are just neutralizing the RNA molecule [Figs. 2(a)–2(c)], the binding-pocket groove becomes narrower and narrower from Na^+ to K^+ to Mg^{2+}. Na^+ ions mainly distribute at the

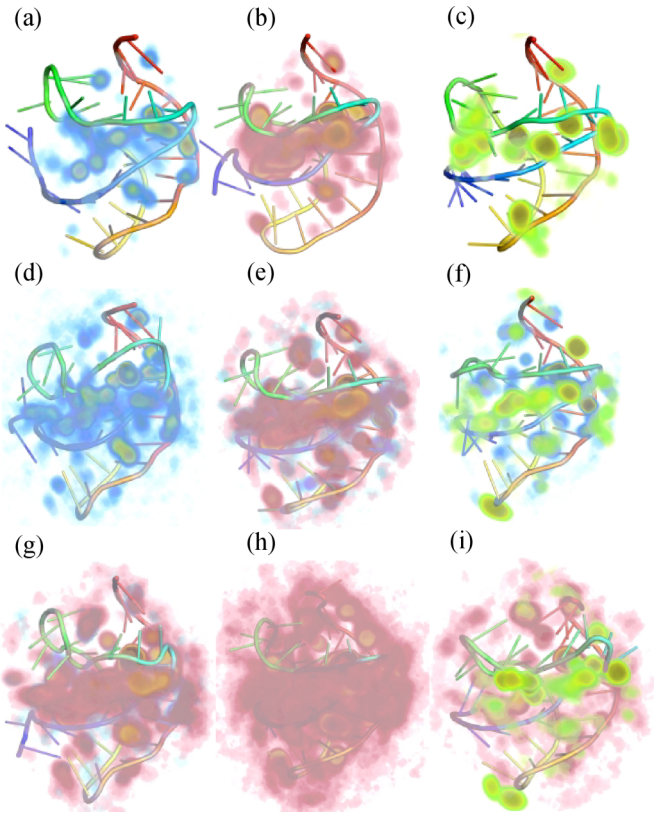

FIG. 2. The distribution of metal ions in different ion conditions. The distribution of sodium ions, potassium ions, and magnesium ions are colored in blue, red, and green, respectively. The dark color in the figure shows the positions where the ions remain for a long time. (a)–(c) are solutions with neutralizing Na^+,K^+, and Mg^{2+} ions, respectively; (d)–(f) are solutions with neutralizing Na^+ ions and extra 0.3*M* NaCl, 0.3*M* KCl, and 0.15*M* $MgCl_2$, respectively; (g)–(i) are solutions with neutralizing K^+ ions and extra 0.3*M* NaCl, 0.3*M* KCl, and 0.15*M* $MgCl_2$, respectively.

bottom of the groove [Fig. 2(a)] and interact strongly with P1. This makes P1 and L3 very stable while P2, L1, and L2 are flexible and so have no significant influence on the native shape of the groove [Fig. 4(a)]. On the other hand, since K^+ ions distribute around the opening of the binding-pocket groove [Fig. 2(b)], K^+ ions have stronger interactions with L1, L2, and P1. These interactions not only reduce the flexibility of L1 and L2 but also attract P1 and L2 to become closer. It is noted that this probably weakened the interaction between P1 and L3 and made L3 more flexible [Fig. 4(b)]. In the case of Mg^{2+} ions [Fig. 2(c)], due to their smooth but discrete distribution in the binding-pocket groove and large charges, they have much stronger interactions with L1, L2, and P1 than the K^+ ions and not only further reduce the flexibility of L1 and L2 but also greatly compress the groove [Fig. 2(c)]. This also weakens the interactions between P1 and L3 and between L2 and one of the chains of P2, and leads to L3 and one of the chains of P2 becoming very flexible [Fig. 4(c)].

In the cases of excess salts with 0.3*M* NaCl, 0.3*M* KCl, or 0.15*M* $MgCl_2$ in addition to the net-neutralizing ions, the cations now also have a chance to distribute around other parts of the molecules besides the binding-pocket groove.

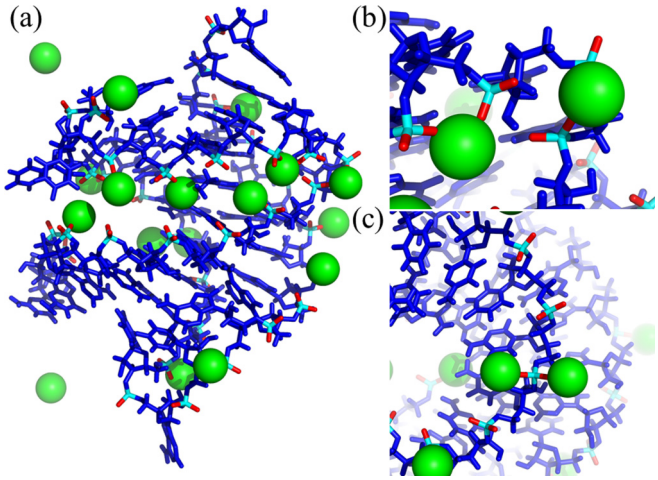

FIG. 3. The distribution of Mg^{2+} ions around the $preQ_1$ riboswitch aptamer domain in a solution with only neutralizing Mg^{2+} ions and their interactions with the backbone phosphate groups. (a) The distribution of Mg^{2+} ions around the $preQ_1$ riboswitch aptamer domain; (b) one Mg^{2+} ion interacts with two phosphate groups; (c) two Mg^{2+} ions interact with one phosphate group. Mg^{2+} ions are represented by the green balls, the entire molecule is in blue, and the oxygen and phosphate atoms of the phosphate groups are in red and cyan, respectively.

Among the six cases only in the solution with neutralizing K^+ and excess 0.3*M* KCl [denoted as K^+-KCl, Fig. 2(h)], the ions now can almost smoothly distribute around the whole molecule and thus balance the effect of the K^+ ions in the binding-pocket groove and keep the native conformations of the groove [Fig. 4(h)]. The case of K^+-NaCl is similar to K^+-KCl [Fig. 2(g)]. In all other cases the metal ions mainly stay in the binding-pocket groove, too, and their effects cannot be balanced by the ions around other parts of the molecule. Therefore, the native conformation of the groove is still compressed (Fig. 2).

The different ion distributions not only affect local structures but also lead to different dynamical behaviors or flexibilities of the molecule. This can be seen from Fig. 4, the RMSD boxplots of the simulated results for the nine ion solutions discussed above, which gives the RMSD distributions of the simulated trajectories of the entire molecule (W), the lower and upper parts (LP and UP), and their components (P1, P2, L1, L2, L3) relative to the first of the NMR structures. In different ion solutions the global structure and flexibility (dynamics) of the molecule are similar but the local dynamics is different. For example, in the solutions with just neutralizing Na^+,K^+, and Mg^{2+} ions [Figs. 4(a)–4(c)], the structures and flexibilities are similar, having RMSD medians of about 3.2, 3.4, and 3.9 Å and RMSD distributions from 2.7 to 4 Å, 2 to 5 Å, and 2.5 to 5.2 Å, respectively; However, their local behaviors are different. In the solution with just neutralizing Na^+ ions [Fig. 4(a)], the LP part as well as P1 and L3 are very stable and L2 and P2 are flexible, as observed experimentally; However, L1 is very flexible and behaves differently from their observed ps–ns time-scale behaviors. In the K^+ ion solution [Fig. 4(b)], the local behaviors of the molecule are different from the case of Na^+ ions: The LP part and also its components P1 and L3

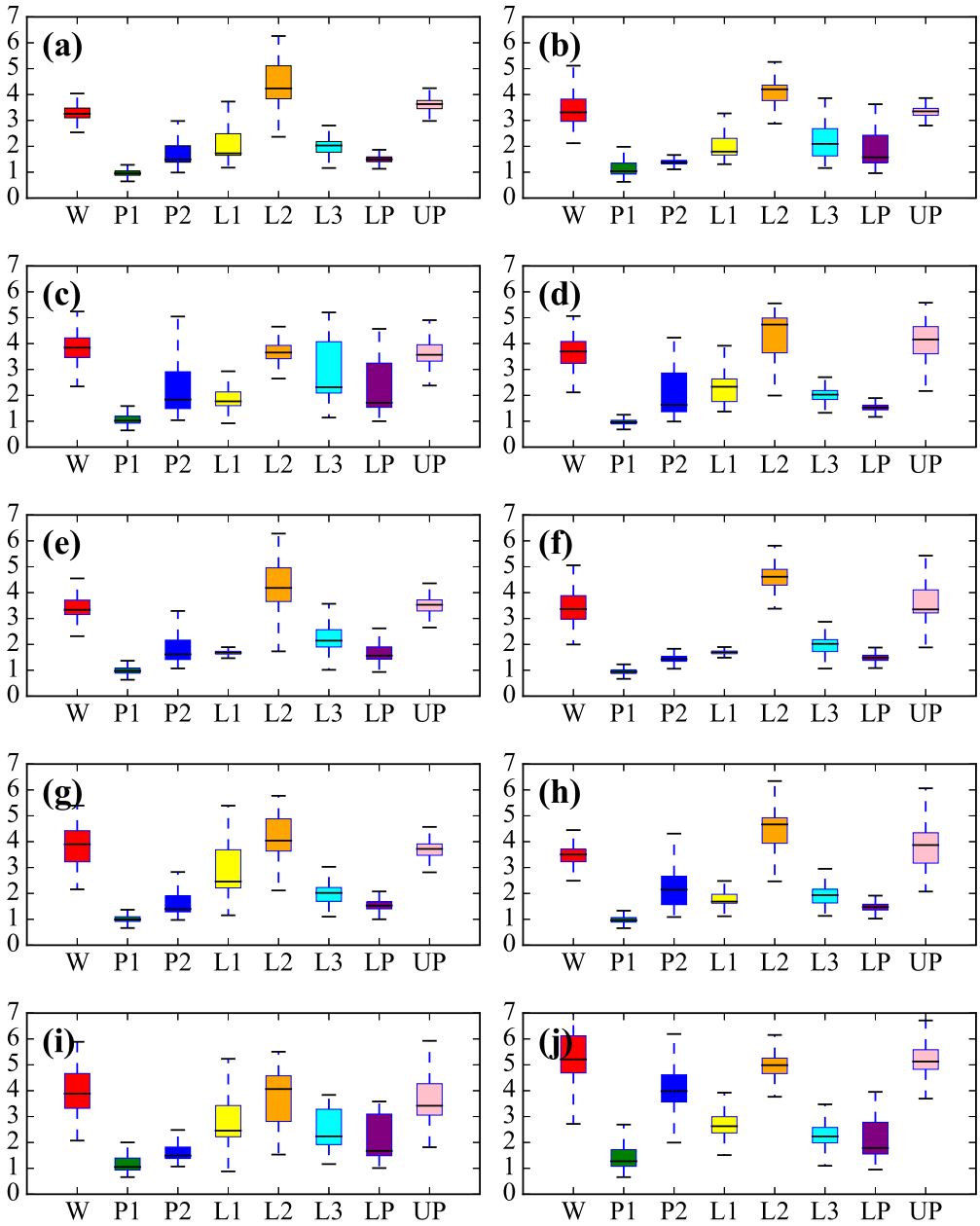

FIG. 4. Boxplot of RMSD of different regions in MD simulations. (a)–(c) are solutions with neutralizing Na^+,K^+, and Mg^{2+} ions, respectively; (d)–(f) are solutions with neutralizing Na^+ ions and extra 0.3M NaCl, 0.3M KCl. and 0.15M $MgCl_2$, respectively; (g)–(i) are solutions with neutralizing K^+ ions and extra 0.3M NaCl, 0.3M KCl, and 0.15M $MgCl_2$, respectively; (j) is the solution without any ions. The lower and upper horizontal line is the minimum and maximum value, respectively. The lower and upper edge of the box is the first and third quantile, respectively. The middle line in the box is the median. "W" denotes the entire molecule.

become more flexible while the UP part and its components P2 and L2 become more stable, which are inconsistent with the observed behaviors of this molecule. For the case of Mg^{2+} ions [Fig. 4(c)], in comparison with the case of K^+ ions, the flexibilities of LP and L3 further increase but those of L1 and L2 decrease. Furthermore, P2 and UP become more flexible, even larger than the case of Na^+ ions.

For excess salt solutions [Figs. 4(d)–4(i)], the situations are similar. In most cases the structures and dynamics of the structures are also similar to the three cases above, but those of some components are different from each other and also from experimental observations. For example, in the cases of Na^+-NaCl and K^+-NaCl, L1 become flexible [Figs. 4(d) and 4(g)]; in the case of Na^+-$MgCl_2$, P2 becomes too stable [Fig. 4(f)]; in the case of K^+-$MgCl_2$, LP and L1 become more flexible [Fig. 4(i)]. However, it is found that in the case of K^+-KCl [Fig. 4(h)], both global and local behaviors of the molecule are in good agreement with the experimental observations on the ps–ns time scale. In this case the part LP and its components P1 and L3 are very stable and the same for L1, while the part UP and its components L2 and P2 are flexible, as observed experimentally. In the solution

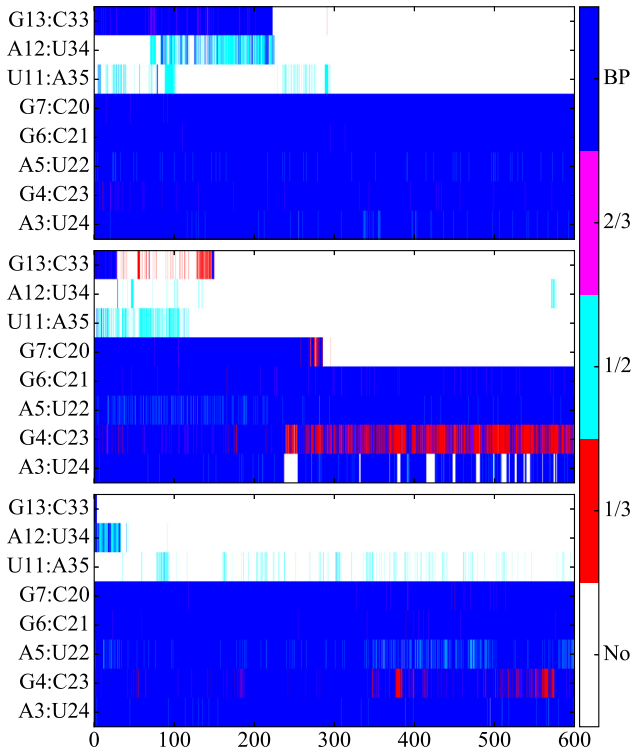

FIG. 5. Hydrogen bond occupancies in three trajectories of molecular dynamics (MD) simulations without any added ions. The blue color represents the unbroken base pair; the purple and red color denotes a G-C base pair with one or two broken hydrogen bonds (H-bond), respectively; the cyan color stands for an A-U base pair with one broken H bond; the white color represents the entirely broken base pairs.

with Na^+-KCl the behavior of the molecule is very similar to the case of K^+-KCl, except that the flexibility of L3 is a little larger [Fig. 4(e)]. Therefore, in all cases the behaviors of the molecule are globally similar but locally different. In most cases the local behaviors are not completely consistent with the observed behaviors of this molecule on a ps–ns time scale.

For comparison, the behaviors of the molecule in the solution without any metal ions are also investigated. In this case [Fig. 4(j)] the entire molecule and all parts have large RMSD values and wide RMSD distributions and the whole system tends to unfold, as expected. For example, the RMSD median of the entire molecule is larger than 5 Å and the RMSD distribution is from 2.8 to 7.5 Å. P2 loses its native conformation and the base pairs break (Fig. 5). The P1 and also LP are also destabilized. These behaviors are in agreement with Draper's results [49,50]. This is the well-known fact that RNA needs cations to balance the strong electronegativity of their backbones in order to keep their structures.

It is interesting to compare the differences in the ion distributions around RNA and DNA. Since the ion distributions depend on the sequences and conformations of nucleic acids, the comparisons were made usually for simple helical conformations and sequences [51]. The conformation of the PRAD is much more complex than pure helical conformations of DNA, and it is also interesting to see the differences in the ion distributions around a complex structure and a pure helical one. In a previous paper the authors studied the ion distributions around B-DNA and A-RNA with the same sequence by using molecular dynamics simulations in an explicit solvent [51]. They found that monovalent ions Na^+ and K^+ were distributed in both major and minor grooves for B-DNA at excess salt but mainly in the major groove A-RNA in this case. Moreover, in B-DNA, the metal ions are more evenly distributed while in RNA they are more localized. They also found that for B-DNA the bivalent ion Mg^{++} was mainly bound to certain oxygens or nitrogens of base pairs but for A-RNA to the backbone phosphate oxygens. For the PRAD, we obtained similar results. These can be seen clearly in Figs. 2(a)–2(f). As discussed above, the monovalent ions Na^+ and K^+ are mainly distributed in the binding-pocket region that contains parts of the major grooves of P1 and P2. Their localization features are shown by the spots of the ion distribution plots. The binding sites of the bivalent ion Mg^{++} can be clearly seen in Fig. 3. Of course, these features of the ion distributions around the PRAD are also determined by its electrostatic surface, which has a large negative charge distribution within the binding pocket (Fig. 1). So, the ions can also distribute in the other part (around L2) of the binding pocket besides the major groove of P1. This phenomenon is due to the complex structure of the PRAD and cannot be seen in the case of pure helical conformation. These features of the ion distributions around the PRAD can significantly affect the local structures as the ion types and concentrations change, even at low ion concentration (Fig. 2). In a previous work [51] the authors also found the structure of A-RNA was affected by the ion concentration, such as helical and step rise and helical inclination, but for the complex structure of the PRAD, we can see that the ion types and concentrations can have strong effects on the structures of larger scales, e.g., the binding pocket. At all, these effects are different from B-DNA whose structure was found to be not very sensitive to the ion concentration.

In summary, we have shown for PRAD that metal ions usually do not distribute uniformly around a RNA molecule with a complex structure, and the distributions depend on ion types and concentrations and the molecular electrostatic surface and lead to different local structures and dynamics of the molecule. For PRAD, in the K^+-KCl solution, similar to the experimental buffers, the molecule captures both global and local behaviors observed experimentally on the ps–ns time scale. Our results also show that the features of ion distributions around complex RNA structures and their effects on the structures are different from those for B-DNA. It is noted that some features of Mg^{2+} ions are not accurately described by the current force fields, e.g., the polarization. Therefore, the effect of Mg^{2+} ions needs further study. Our results may be helpful to understand and correctly model the roles of metal ions on the structure and dynamics of RNA.

This work is supported by the NSFC under Grants No. 11374113 and No. 31570722 and the National High Technology Research and Development Program of China (2012AA020402).

[1] N. A. Denesyuk and D. Thirumalai, Nat. Chem. **7**, 793 (2015).
[2] P. Auffinger, L. D'Ascenzo, and E. Ennifar, Met. Ions Life Sci. **16**, 167 (2016).
[3] Y. Z. Shi, L. Jin, F. H. Wang, X. L. Zhu, and Z. J. Tan, Biophys. J. **109**, 2654 (2015).
[4] Z. Tan, W. Zhang, Y. Shi, and F. Wang, Adv. Exp. Med. Biol. **827**, 143 (2015).
[5] Y. Zhu, Z. He, and S. J. Chen, PloS One **10**, e0119705 (2015).
[6] A. E. Johnson-Buck, S. E. McDowell, and N. G. Walter, Met. Ions Life Sci. **9**, 175 (2011).
[7] A. R. Ferre-D'Amare and W. C. Winkler, Met. Ions Life Sci. **9**, 141 (2011).
[8] Q. Zhang, M. Kang, R. D. Peterson, and J. Feigon, J. Am. Chem. Soc. **133**, 5190 (2011).
[9] R. L. Hayes, J. K. Noel, A. Mandic, P. C. Whitford, K. Y. Sanbonmatsu, U. Mohanty, and J. N. Onuchic, Phys. Rev. Lett. **114**, 258105 (2015).
[10] Z. Gong, Y. Zhao, C. Chen, and Y. Xiao, PloS One **7**, e45239 (2012).
[11] L. Z. Sun and S. J. Chen, J. Chem. Theory Comput. **12**, 3370 (2016).
[12] D. Leipply and D. E. Draper, Biochemistry **50**, 2790 (2011).
[13] M. Kang, R. Peterson, and J. Feigon, Mol. Cell **33**, 784 (2009).
[14] J. Buck, J. Noeske, J. Wohnert, and H. Schwalbe, Nucleic Acids Res. **38**, 4143 (2010).
[15] D. J. Klein, T. E. Edwards, and A. R. Ferre-D'Amare, Nat. Struct. Mol. Biol. **16**, 343 (2009).
[16] Y. Liu, T. J. Wilson, S. A. McPhee, and D. M. Lilley, Nat. Chem. Biol. **10**, 739 (2014).
[17] G. Desjardins, E. Bonneau, N. Girard, J. Boisbouvier, and P. Legault, Nucleic Acids Res. **39**, 4427 (2011).
[18] M. V. Schrodt, C. T. Andrews, and A. H. Elcock, J. Chem. Theory Comput. **11**, 5906 (2015).
[19] K. Réblová, Z. Střelcová, P. Kulhánek, I. Beššeová, D. H. Mathews, K. V. Nostrand, I. Yildirim, D. H. Turner, and J. Šponer, J. Chem. Theory Comput. **6**, 910 (2010).
[20] X. Xue, W. Yongjun, and L. Zhihong, J. Theor. Biol. **365**, 265 (2015).
[21] V. Mlynsky, P. Kuhrova, M. Zgarbova, P. Jurecka, N. G. Walter, M. Otyepka, J. Sponer, and P. Banas, J. Phys. Chem. B **119**, 4220 (2015).
[22] Z. Gong, Y. Zhao, C. Chen, Y. Duan, and Y. Xiao, PloS One **9**, e92247 (2014).
[23] Z. Gong, Y. Zhao, C. Chen, and Y. Xiao, J. Biomol. Struct. Dyn. **29**, 403 (2011).
[24] O. Allner, L. Nilsson, and A. Villa, RNA **19**, 916 (2013).
[25] J. Wang, Y. Zhao, J. Wang, and Y. Xiao, Phys. Rev. E **92**, 062705 (2015).
[26] Z. Gong, Y. Xiao, and Y. Xiao, J. Biomol. Struct. Dyn. **28**, 431 (2010).
[27] P. Banas, N. G. Walter, J. Sponer, and M. Otyepka, J. Phys. Chem. B **114**, 8701 (2010).
[28] W. L. DeLano, M. H. Ultsch, and J. A. Wells, Science **287**, 1279 (2000).
[29] R. Salomon-Ferrer, D. A. Case, and R. C. Walker, Wiley Interdiscip. Rev.: Comput. Mol. Sci. **3**, 198 (2013).
[30] L. C. Pierce, R. Salomon-Ferrer, C. Augusto, F. de Oliveira, J. A. McCammon, and R. C. Walker, J. Chem. Theory Comput. **8**, 2997 (2012).
[31] R. Salomon-Ferrer, A. W. Goötz, D. Poole, S. Le Grand, and R. C. Walker, J. Chem. Theory Comput. **9**, 3878 (2013).
[32] D. A. Case, V. Babin, J. T. Berryman, R. M. Betz, Q. Cai, D. S. Cerutti, T. E. Cheatham III, T. A. Darden, R. E. Duke, H. Gohlke, A. W. Goetz, S. Gusarov, N. Homeyer, P. Janowski, J. Kaus, I. Kolossváry, A. Kovalenko, T. S. Lee, S. LeGrand, T. Luchko, R. Luo, B. Madej, K. M. Merz, F. Paesani, D. R. Roe, A. Roitberg, C. Sagui, R. Salomon-Ferrer, G. Seabra, C. L. Simmerling, W. Smith, J. Swails, R. C. Walker, J. Wang, R. M. Wolf, X. Wu, and P. A. Kollman, *AMBER 14* (University of California, San Francisco, 2014).
[33] A. Pérez, I. Marchán, D. Svozil, J. Sponer, T. E. Cheatham, C. A. Laughton, and M. Orozco, Biophys. J. **92**, 3817 (2007).
[34] M. Zgarbová, M. Otyepka, J. I. Šponer, A. T. Mládek, P. Banáš, T. E. Cheatham III, and P. Jurecka, J. Chem. Theory Comput. **7**, 2886 (2011).
[35] J. Wang, W. Wang, P. A. Kollman, and D. A. Case, J. Mol. Graphics Modell. **25**, 247 (2006).
[36] J. Wang, R. M. Wolf, J. W. Caldwell, P. A. Kollman, and D. A. Case, J. Comput. Chem. **25**, 1157 (2004).
[37] A. Jakalian, B. L. Bush, D. B. Jack, and C. I. Bayly, J. Comput. Chem. **21**, 132 (2000).
[38] D. A. Case, T. E. Cheatham, T. Darden, H. Gohlke, R. Luo, K. M. Merz, A. Onufriev, C. Simmerling, B. Wang, and R. J. Woods, J. Comput. Chem. **26**, 1668 (2005).
[39] I. S. Joung and T. E. Cheatham III, J. Phys. Chem. B **112**, 9020 (2008).
[40] P. Li, B. P. Roberts, D. K. Chakravorty, and K. M. Merz, Jr., J. Chem. Theory Comput. **9**, 2733 (2013).
[41] J.-P. Ryckaert, G. Ciccotti, and H. J. C. Berendsen, J. Comput. Phys. **23**, 327 (1977).
[42] R. J. Loncharich, B. R. Brooks, and R. W. Pastor, Biopolymers **32**, 523 (1992).
[43] U. Essmann, L. Perera, M. L. Berkowitz, T. Darden, H. Lee, and L. G. Pedersen, J. Chem. Phys **103**, 8577 (1995).
[44] D. R. Roe and T. E. Cheatham III, J. Chem. Theory Comput. **9**, 3084 (2013).
[45] J. D. Hunter, Comput. Sci. Eng. **9**, 90 (2007).
[46] R. Ihaka and R. Gentleman, J. Comput. Graph. Stat. **5**, 299 (1996).
[47] L. Li, C. Li, S. Sarkar, J. Zhang, S. Witham, Z. Zhang, L. Wang, N. Smith, M. Petukh, and E. Alexov, BMC Biophys. **5**, 9 (2012).
[48] K. S. Kim and E. Clementi, J. Am. Chem. Soc. **107**, 5504 (1985).
[49] D. E. Draper, Biophys. J. **95**, 5489 (2008).
[50] D. E. Draper, A. M. Soto, and V. Misra, Biochemistry **46**, 2973 (2007).
[51] F. Pan, C. Roland, and C. Sagui, Nucleic Acids Res. **42**, 13981 (2014).